JOURNAL OF AIRCRAFT
Vol. 45, No. 4, July–August 2008

Computational Prediction of Roll Damping for the F/A-18E at Transonic Speeds

Bradford E. Green*
Naval Air Systems Command, Patuxent River, Maryland 20670

DOI: 10.2514/1.34571

Computational fluid dynamics was used to predict the roll-damping characteristics for the F/A-18E Super Hornet at transonic speeds. The calculations were made for Mach 0.8 at both wind-tunnel and flight conditions. Three different wing configurations were analyzed during this study. For the first two configurations, the F/A-18E Super Hornet was modeled with the preproduction wing. The first of these configurations had flap settings of 6 degree leading-edge flaps, 8 degree trailing-edge flaps, and 4 degree aileron, whereas the second configuration had flap settings of 10 degree leading-edge flaps, 10 degree trailing-edge flaps, and 5 degree aileron. The third configuration analyzed was that of the F/A-18E with the wing developed from the Transonic Flying Qualities Improvement Program. This wing includes a sawtooth leading edge and a chordwise fence on the wing box. The sawtooth geometry eliminated the snag that existed on the leading edge of the preproduction wing. The flow solver of the NASA Tetrahedral Unstructured Software System was used during this project. In preparation for this study, the flow solver was modified to simulate a constant-rate rolling motion of the grid so that the roll-damping characteristics of the aircraft could be determined. With this modification to the flow solver, the roll-damping characteristics at each condition could be determined at the expense of a steady-state computational fluid dynamics calculation. This approach to determining roll damping is much simpler and faster than the traditional approach, which required a time-accurate calculation on a moving grid. The results of this study indicate that computational fluid dynamics can be a useful analysis tool for screening a configuration for potential loss of roll damping and the associated deterioration of lateral handling qualities.

Nomenclature

b	=	wing span, ft
$C_{l_{\dot{\beta}}}$	=	rolling-moment coefficient due to rate of change of sideslip
C_{l_p}	=	rolling-moment coefficient due to roll rate
c_l	=	section-lift coefficient
p	=	roll rate, deg/s
Re_c	=	Reynolds number based on mean aerodynamic chord
y	=	dimension in spanwise direction, ft
α	=	angle of attack, deg
β	=	angle of sideslip, deg
$\dot{\beta}$	=	rate of change of sideslip, deg/s
δ_s	=	horizontal-tail deflection angle, deg

I. Introduction

THE analysis of stability-and-control (S&C) characteristics of high-performance fighter aircraft involves prediction of behavior at and beyond the edge of the flight envelope at transonic speeds. At these conditions, aerodynamic characteristics are difficult to predict due to massive shock-induced flow separation, nonlinear aerodynamics, effects of aircraft dynamic motions, and time-dependent phenomena. Traditionally, wind tunnels have been used by the S&C community to predict, analyze, and resolve the characteristics of aircraft in this difficult flow regime. Wind tunnels, however, have limitations (Reynolds number, for example) and sometimes cannot accurately predict the aerodynamic characteristics of the aircraft. Although computational fluid dynamics (CFD) could theoretically be used to model aircraft aerodynamics at flight conditions at and beyond the edge of the envelope, CFD has not yet been fully calibrated and proven for these conditions. This computational effort represents an initial exploratory investigation into using CFD for predicting the S&C characteristics of aircraft for such conditions.

Because of the inherent difficulty in accurately predicting the S&C characteristics of an aircraft at the edge of the flight envelope, nearly every advanced aircraft program has been surprised by unpredicted, undesirable aerodynamic phenomena [1]. Eliminating these undesirable characteristics is both costly and time consuming, due to the amount of wind-tunnel testing and "cut and try" flight testing involved. Obviously, it is more desirable to accurately predict and fix problems early in a development program. Although CFD could be used in conjunction with wind-tunnel tests to find potential problems, S&C engineers are currently not trusting CFD due to the lack of applications and calibrations of the codes for their area of expertise. CFD has been used with success to predict the aerodynamic performance of aircraft and for flow diagnostics, but CFD has not been widely used for force and moment calculations for S&C. This "gap" between the traditional uses of CFD and the needs of the S&C community has made it difficult for CFD users to earn the support of the S&C engineers. In addition, lack of exposure to the problems faced by S&C engineers has resulted in CFD experts being uninformed as to the opportunities and contributions that they might make to the state of the art.

As a result of the gap in communications and lack of partnerships between CFD users and the S&C community, NASA, with participation from the U.S. Department of Defense (DoD) and industry, started plans for a Computational Methods for Stability and Control (COMSAC) program in 2003. The COMSAC program was formed to focus CFD tools to applications in S&C and to improve communications between CFD and S&C specialists. In September 2003 in Hampton, Virginia, the COMSAC program brought together over 100 CFD experts and S&C engineers from government and industry to share their present and future needs.

Stimulated by the COMSAC initiative, a project within the Common High Performance Computing Software Support Initiative (CHSSI) is dedicated to evaluating and improving CFD codes that might quickly and accurately predict the S&C characteristics of

Received 13 September 2007; revision received 1 November 2007; accepted for publication 11 November 2007. This material is declared a work of the U.S. Government and is not subject to copyright protection in the United States. Copies of this paper may be made for personal or internal use, on condition that the copier pay the $10.00 per-copy fee to the Copyright Clearance Center, Inc., 222 Rosewood Drive, Danvers, MA 01923; include the code 0021-8669/08 $10.00 in correspondence with the CCC.

*Aerospace Engineer, Applied Aerodynamics and Stores Separation Branch, Building 2187, Unit 5, Suite 1320-B, 48110 Shaw Road. Senior Member AIAA.

complex aircraft configurations at challenging flight conditions. This project, named Integrated Simulation of Air Vehicle Performance, Stability and Control for Test and Evaluation, is within the Collaborative Simulation and Testing (CST) Integrated Portfolio. This project is composed of engineers from the Naval Air Systems Command, NASA Langley, the U.S. Air Force Research Laboratory, and several contractors and consultants.

The exploratory CFD calculations performed as part of the CST portfolio have been conducted in three phases. In the first phase of the project, CFD was used to predict the static longitudinal and lateral/directional S&C characteristics of the preproduction F/A-18E at two transonic Mach numbers. The results of this work are presented in their entirety in [2]. The correlation of CFD with the wind-tunnel data was generally very good. More work is required, however, to analyze differences apparently caused by effects of complex aerodynamic unsteadiness near wing stall. The agreement between the CFD results and the wind-tunnel data for the longitudinal S&C characteristics was good, although the agreement near wing stall was poor. The general character of the longitudinal control effectiveness was predicted reasonably well by the code. For the most part, CFD did an exceptional job of predicting the lateral/directional S&C characteristics of the aircraft at the transonic conditions. At wing stall, large differences existed between results from two wind tunnels as well as CFD. Above wing stall at Mach 0.9, the CFD results were dependent upon the initial condition of the calculation because of the unsteady nature of the flow. Redoing the calculations with different initial conditions resulted in good agreement between wind tunnel and CFD.

In the second phase of the project, CFD was used to predict the longitudinal S&C characteristics of the preproduction F/A-18E with neutral and full nose-down control at low-speed, high-angle-of-attack conditions. The results of this work are presented in [3]. Calculations were performed for Mach 0.082 for angles of attack between 0 and 60 deg. Initially, the Spalart–Allmaras (SA) turbulence model was used. The CFD results using SA correlated well with the wind-tunnel data for angles of attack below $\alpha = 40$ deg. Above 40 deg, however, the CFD results differed from the wind-tunnel data. Despite the poor correlation at the higher angles of attack, the tail effectiveness was accurately predicted for angles of attack between 0 and 60 deg. An improved correlation with the wind-tunnel data was achieved at $\alpha = 60$ deg using Menter's shear stress transport model.

The third, and final, phase of the CFD calculations performed during the CST portfolio will be presented in this paper. In this phase of the project, the goal was to assess the ability of CFD to predict the aerodynamic roll-damping characteristics of the F/A-18E Super Hornet at transonic speeds. Roll-damping characteristics can determine a number of critical lateral handling qualities, including wing drop, wing rock, and nonlinear response to control inputs. Therefore, an accurate prediction of roll damping is a highly desirable capability in early design stages. Prediction of aerodynamic roll damping for transonic, separated-flow conditions is particularly difficult. The aerodynamic behavior of contributing factors can be highly nonlinear with rate of roll, discontinuous or time dependent, as well as other ill-behaved trends. In addition, the extraction of values of roll damping from flight data is very challenging because of large-amplitude motions, lack of repeatability in some maneuvers, and possible uncontrollable maneuvers. If CFD can augment the conventional tools used to predict roll damping, it could become a major advance in the state of the art.

Before starting the computations, the USM3D flow solver was modified to include a rolling swirl component of the velocity about the wind axis of the aircraft. With this modification, the aircraft would be effectively rolling at a constant rate about the wind axis and the roll-damping characteristics of the aircraft could be estimated at the expense of a steady-state CFD calculation. Although the results would be compared with an aircraft that is rolling about the body axis instead of the wind axis, only low angles of attack would be considered and the difference in roll damping that result would be expected to be small.

The CFD calculations were performed for Mach 0.8 at both wind-tunnel and flight conditions. Although the majority of the calculations were completed for a roll rate of 20 deg/s, a few of the calculations were performed at a roll rate of 90 deg/s in an effort to demonstrate that CFD would predict the anticipated nonlinear trend of roll damping with roll rate. Where possible, the calculations that were performed for wind-tunnel conditions were compared with existing wind-tunnel "free-to-roll" test data. As will be discussed in this paper, it is technically incorrect to make a direct one-to-one comparison between the roll damping from the present CFD study and the roll damping from the free-to-roll wind-tunnel test, but the comparison indicates the effectiveness of CFD for assessing the roll-damping characteristics of an aircraft. In an effort to illustrate the differences in roll damping between wind-tunnel and flight conditions, some of the CFD calculations were also conducted for flight conditions.

Three different F/A-18E configurations were considered during this project. The first configuration was that of the preproduction F/A-18E with 6/8/4 flaps (6 deg leading-edge flaps, 8 deg trailing-edge flaps, and 4 deg aileron deflection). This configuration was known to experience abrupt wing stall (AWS) [4] and would be a well-known F/A-18E characteristic for which CFD could be evaluated. The second configuration was the preproduction F/A-18E with 10/10/5 flaps. The abrupt-wing-stall characteristics of this configuration were known to be less severe than those of the configuration with 6/8/4 flaps. The final configuration was that of the preproduction F/A-18E with 10/10/5 flaps and a sawtooth and chordwise fence on the wing. Based on flight tests, this configuration should have very little tendency toward abrupt wing drop or unstable roll motions. The CFD calculations were performed "blind," without prior knowledge of the existing wind-tunnel data.

In the following section, the grid generator and flow solver used during this study are discussed. A description of the geometry and grids is included in the subsequent section. The computer requirements are then discussed, followed by results and discussion of the roll-damping estimation methods of CFD and free-to-roll wind-tunnel testing. In the next section, the results of the computational study are presented. Finally, some conclusions of the study are offered.

II. Discussion of Grid Generator and Flow Solver

The NASA Tetrahedral Unstructured Software System (TetrUSS) [5] was used to analyze the aerodynamics and lateral S&C characteristics of the preproduction F/A-18E during this study. TetrUSS consists of a loosely integrated, user-friendly set of software tools composed of a geometry setup tool GridTool, a tetrahedral grid generator VGRID, a tetrahedral Navier–Stokes flow solver USM3D, and several pre- and postprocessing utility tools.

A. VGRID Grid Generator

VGRID is a computer program for automatic generation of tetrahedral unstructured grids suitable for computing Euler and Navier–Stokes flow solutions. The methodology is based on an integration of the advancing-layers method (ALM) [6] and advancing-front method (AFM) [7]. VGRID can generate multidirectional, anisotropic stretched grids in which the surface triangles and tetrahedra in the field are elongated in user-prescribed directions. Information regarding the unstructured grid point distribution is provided to the AFM and ALM marching processes by a "transparent" background grid overlaying the entire domain. Recent extensions to VGRID have included the addition of both surface and volume sources that result in significantly better grid control and quality.

The input data to VGRID is set up in the GridTool [8] code. The user constructs a number of contiguous surface patches over the underlying initial graphics exchange specification (IGES) surface definition. The grid characteristics such as spacing sources, stretching parameters, rate of growth, etc., are also prescribed by the user with GridTool to complete the input data file.

B. USM3D Flow Solver

USM3D [9] is a tetrahedral cell-centered, finite volume Euler and Navier–Stokes (N-S) flow solver. Inviscid flux quantities can be computed across each cell face with a variety of upwind flux functions. The solution is advanced in time by an implicit backward-Euler time-stepping scheme with local time-stepping convergence acceleration for steady-state problems. The most recent enhancements to USM3D are second-order time accuracy with detached eddy simulation [10], boundary-layer flow tripping [11], and dynamic grid motion dynamic overset-grid modification [12].

USM3D has several closure models for capturing flow turbulence effects. First is the Spalart–Allmaras one-equation model [13], which can be coupled with a wall function boundary condition to reduce the number of cells in the sublayer region of the boundary layer. However, the wall function boundary condition is typically used only when extensive curvature-based separation is not expected in a flow simulation. Several two-equation turbulence models are also available, such as the Jones and Launder linear k-epsilon model [14,15], the Menter shear stress transport (SST) model [16], and two nonlinear algebraic Reynolds stress models (ARSM) by Girimaji [17] and by Shih et al. [18]. Some of these turbulence models have undergone testing on propulsion afterbody flows [19].

USM3D supports an array of useful boundary conditions (BCs). It contains the standard BCs of flow tangency or no-slip on solid surfaces, characteristic inflow/outflow for subsonic boundaries, and freestream inflow and extrapolation outflow for supersonic flow. Some additional special BCs are also available for jet exhaust and intake, a propeller/rotor actuator disk model, and passive porosity.

USM3D runs on massively parallel computers and clusters of personal computers. A grid-partitioning file is quickly generated during a preprocessing step with a customized version of the Metis code [20] file. Thus, the user may readily change the number of processors from one restart run to the next if desired.

C. Extension of USM3D for Constant-Rate Roll Capability

USM3D was extended for this study to include capability for computing roll-damping coefficients on a stationary grid using a steady-state calculation. These extensions were made by Neal T. Frink of NASA Langley Research Center, Hampton, Virginia and Mohagna J. Pandya of Analytical Services and Materials, Hampton, Virginia. This extension follows the approach by Park and Kwon [21] for adding noninertial source terms and accompanying grid-speed terms to the Navier–Stokes equations for simulating a constant-rate rolling motion about the wind axis in a stationary reference frame. This formulation simulates a body rotating at a constant rate about the wind axis without physically rotating the grid.

The underlying assumption of rotation about the wind axis is restrictive for general motion. However, the abrupt-wing-stall phenomenon occurred on the preproduction F/A-18E at relatively low angles of attack in the range of 7–8 deg. Hence, the small angle assumption is applied to the present computations at small nonzero angles of attack. In the strictest sense, a coning motion is being modeled in the present work, with the assumption that the roll-damping coefficients are close to those from rolling about the body axis.

III. Geometry and Grid Descriptions

A. Geometry Description

The basic F/A-18E geometry that was analyzed during this study is shown in Fig. 1. The geometry includes a vertical tail, horizontal tail, wing-tip missile and launcher, and a flow-through inlet and duct. Three different wing configurations were considered during this study. These wing configurations are shown in Fig. 2. For the first two configurations, the preproduction wing was used. The flap settings for these configurations are 6/8/4 flaps (6 deg leading-edge flaps, 8 deg trailing-edge flaps, and 4 deg aileron down) and 10/10/5 flaps. The third wing configuration is that from the Transonic Flying Qualities Improvement (TFQI) program with 10/10/5 flaps. As described previously, the TFQI wing differs from the preproduction wing in that the snag has been replaced with a sawtooth geometry and a chordwise fence has been added at BL152.

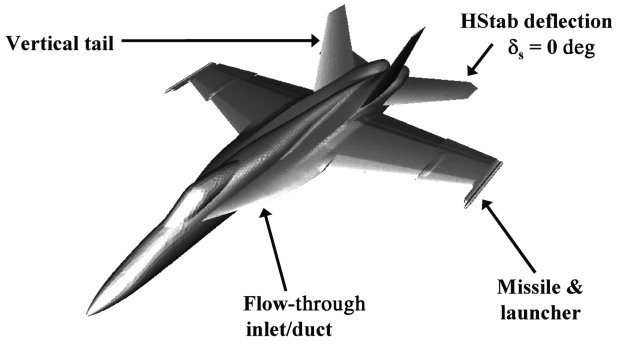

Fig. 1 Computational geometry of the preproduction F/A-18E Super Hornet considered during this study.

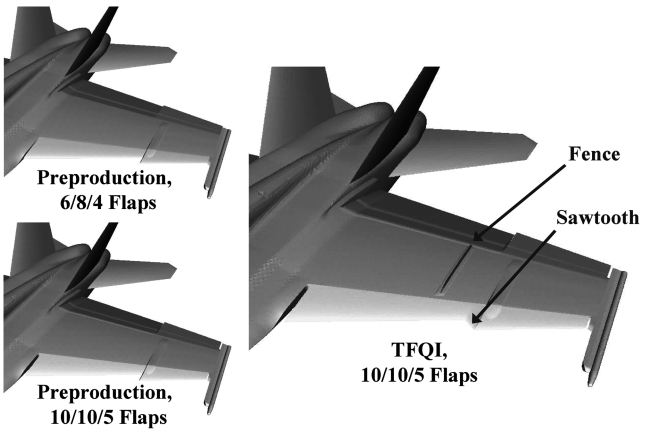

Fig. 2 Three different wing configurations that were analyzed during this study.

B. Grid Descriptions

Seven different computational grids were used during this project. One of the grids was a half-span grid that was used to simulate symmetric flight conditions (longitudinal motions) at zero roll rate. This grid implemented a symmetry-plane boundary condition. Six of the grids were full-span grids that were used to calculate the roll-damping characteristics of the aircraft. All of the grids generated during this study had viscous tetrahedral cells near the surface and inviscid tetrahedral cells away from the surface. The y-plus value of the first cell above the surface was approximately unity for each of the grids. Four of the grids were generated for calculations at wind-tunnel conditions, whereas two of the grids were generated for use at flight conditions.

1. Grids of the Preproduction Aircraft with 6/8/4 Flaps

Four different grids of the preproduction aircraft with 6/8/4 flaps were generated. Two of the grids were full-span configurations with 16.2 and 31.9 million cells, applicable for calculations at wind-tunnel conditions. The grid with 31.9 million cells was generated only for use in a grid-resolution study. Another full-span grid with 16.5 million cells was generated for calculations at flight conditions. The fourth grid was a half-span grid with 8.1 million cells which was used for calculations for symmetric motions at wind-tunnel conditions.

2. Grids of the Preproduction Aircraft with 10/10/5 Flaps

One grid of the preproduction aircraft with 10/10/5 flaps was generated. This was a full-span grid with 18.0 million cells, applicable to wind-tunnel conditions.

Table 1 Number of solutions and CPU requirements for the roll-damping study

Configuration	Grid size, millions	Number of solutions	CPU time, h
Preproduction, 6/8/4 flaps, half-span, wind-tunnel conditions	8.1	13	40,000
Preproduction, 6/8/4 flaps, full-span, wind-tunnel conditions	16.2	30	235,000
Preproduction, 6/8/4 flaps, full-span, wind-tunnel conditions	31.9	1	11,000
Preproduction, 6/8/4 flaps, full-span, flight conditions	16.5	14	127,000
Preproduction, 10/10/5 flaps, full-span, wind-tunnel conditions	18.0	18	157,000
TFQI, 10/10/5 flaps, full-span, wind-tunnel conditions	25.9	17	317,000
TFQI, 10/10/5 flaps, full-span, flight conditions	26.5	17	253,000

3. Grids of the Transonic Flying Qualities Improvement Aircraft with 10/10/5 Flaps

Two different full-span grids of the TFQI aircraft with 10/10/5 flaps were generated. These grids had 25.9 and 26.5 million cells and were generated for calculations at wind-tunnel and flight conditions, respectively.

IV. Computer Requirements

The calculations presented in this paper were performed on SGI Origin 3800/3900 machines available through the DoD High Performance Computing Modernization Office (HPCMO). Each case was run using 128 processors. Table 1 shows the computer-time utilization for each grid.

V. Overview of CFD and Wind-Tunnel Roll-Damping Estimation Methods

A. CFD Estimation Methods

When an aircraft experiences an uncommanded lateral motion during flight, the aircraft rolls about its body axis and the angle of attack, angle of sideslip, rate of change of sideslip, and roll rate change with time. Predicting this behavior accurately with CFD methods would involve time-accurate calculations on moving grids. These calculations would require the latest advances of CFD research and significant computational resources. The present method offers a simpler, faster approach to modeling the lateral characteristics of a rolling aircraft. In the current approach, as previously discussed, USM3D is imposing a rolling swirl of the airstream about the wind axis in an attempt to model the effects of an aircraft spinning about its body axis. Because swirl about the wind axis is being prescribed, the aircraft is effectively experiencing a coning motion, rather than a pure roll about the body axis. It is important to note that the calculations being performed here are steady state and that the grid is stationary. At low angles of attack, the kinematic differences between a roll about the wind axis and the body axis are relatively small, giving a good estimation of the roll-damping coefficient. Because the aircraft is "rolling" about the wind axis, the angle of attack, angle of sideslip, and the rate of sideslip of the aircraft remains fixed during the computation. Specifically, the angle of sideslip was 0 deg and the rate of sideslip was 0 deg/s for the calculations performed during this study.

In performing the roll-damping calculations with CFD, a roll rate is prescribed and is constant for the given calculation. An arbitrary, relatively low roll rate of 20 deg/s was used for the majority of the calculations performed during this study. It was anticipated that any roll instabilities would be detectable with this roll rate.

B. Free-to-Roll Wind-Tunnel Estimation Methods

In this section, the approach to estimating roll damping during free-to-roll wind-tunnel tests will be discussed and the differences between this method and that of CFD will be emphasized. For ease of comparison, the differences in estimation techniques between CFD and the wind tunnel are summarized in Table 2. Owens et al. [4,22] give a good description of the estimation of roll damping from free-to-roll tests in the wind tunnel and Capone et al. [23] give a good description of the details of free-to-roll wind-tunnel test techniques.

During free-to-roll wind-tunnel testing, the aircraft is free to roll about the body axis. This degree of freedom is in contrast to the roll about the wind axis that is imposed in the CFD model. The difference in roll axis between the CFD and free-to-roll wind-tunnel approach is illustrated in Fig. 3. Although the roll axis is different, this discrepancy is not expected to significantly impact the results at low angles of attack.

Table 2 Differences in roll-damping estimation methods between CFD and the wind tunnel

	CFD	Wind tunnel
Roll axis	wind axis	body axis
Roll rate, fixed or varying	fixed	variable
Roll rate, magnitude	low	high
Angle of attack	fixed	variable
Angle of sideslip	0	variable
Rate of sideslip	0	variable
Steady or unsteady	steady	unsteady
Parameter being predicted	C_{l_p}	$C_{l_p} + C_{l_{\dot{\beta}}} \sin\alpha$

During wind-tunnel testing, model motions generate time-dependent variations of roll rate, angle of attack, angle of sideslip, and rate of sideslip. These variations are in contrast to the CFD approach, in which each of these parameters is fixed. As mentioned before, the angle of sideslip was 0 deg and the rate of sideslip was 0 deg/s for the CFD calculations, whereas both parameters were nonzero during the wind-tunnel test. Furthermore, the roll rate chosen for the CFD calculations was much lower than the roll rates encountered during the wind-tunnel test. These differences between CFD and wind tunnel are important and could cause significant discrepancies between the results.

Only steady-state CFD calculations were performed during this study, although the transonic flow over the F/A-18E is inherently unsteady. As a result, the CFD results did not account for the unsteadiness of the flow, whereas the wind-tunnel model would experience the inherent unsteadiness. These differences could also be significant in the AWS range of angles of attack.

Finally, the parameter $C_{l_p} + C_{l_{\dot{\beta}}} \sin\alpha$ is being extracted from the wind-tunnel test using a classic math model [4,22]. Unfortunately, it is not possible to extract only C_{l_p} from the wind-tunnel data. Based on the motion of the aircraft, it is expected that both C_{l_p} and $C_{l_{\dot{\beta}}}$ are nonzero. On the other hand, it is possible to extract only C_{l_p} from the CFD calculations performed during this study. In doing this, however, β was fixed at 0 deg. This makes it difficult to directly

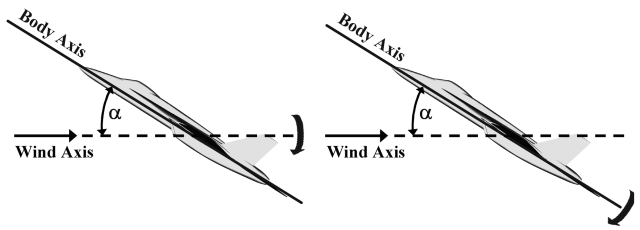

Fig. 3 Illustration of roll axis for roll-damping estimation for CFD, wind tunnel, and flight.

compare the results from CFD to the results from the wind-tunnel test. For purposes of correlation, however, C_{l_p} from CFD will be compared with $C_{l_p} + C_{l_{\dot{\beta}}} \sin\alpha$ from the wind-tunnel test. It is recognized that this comparison is not ideal and does not represent a one-to-one comparison, but this is the best comparison that can be made given the assumptions made in the current CFD calculations. A potential area of future research would include the development of a computational method that would more closely represent what is happening in the wind tunnel and provide a better one-to-one comparison between the CFD and free-to-roll wind-tunnel results.

C. Summary of Differences

As discussed before, there are many differences between the roll-damping estimation methods of CFD and the wind tunnel. For the reasons listed previously, it is impossible to make a one-to-one comparison between the roll-damping results from CFD to the results of the wind-tunnel test. However, trends noted in the CFD results might be indicative of experimental results and useful in further analysis of potential loss of roll damping. Although the roll-damping results from free-to-roll testing should be viewed as a better prediction of what might happen in flight, CFD is a useful tool for predicting the presence of undesirable lateral issues and examining the impact of variables that might not be simulated properly in the wind tunnel, such as values of Reynolds number associated with flight. When undesirable lateral issues are predicted using CFD as a screening and diagnostic tool, it is recommended that these issues be further investigated using free-to-roll wind-tunnel testing.

VI. Results

A. Preproduction F/A-18E with 6/8/4 Flaps at Wind-Tunnel Conditions

The roll-damping characteristics of the preproduction F/A-18E with 6/8/4 flaps were calculated using USM3D for Mach 0.8 and a wind-tunnel Reynolds number based on the mean aerodynamic chord (MAC) of 3.9 million for angles of attack between 0 and 12 deg. This configuration is known to exhibit characteristics of abrupt wing stall and large uncommanded roll-off motions [4], and these characteristics should be evident in the roll-damping characteristics of the aircraft. These calculations were conducted for a roll rate of 20 deg/s. In Fig. 4, the roll-damping coefficients from CFD are plotted as a function of angle of attack for the grids with 16.2 and 31.9 million cells. A single calculation for the grid with 31.9 million cells was performed at $\alpha = 0$ deg to show that the roll-damping coefficient is independent of grid size. In this plot, negative (stable) values of roll-damping derivative are plotted in the top half of the plot and positive (unstable) values of roll damping are plotted in the bottom half of the plot. As would be expected, the roll-damping coefficients at the lower angles of attack are stable, indicating an aircraft with satisfactory roll damping. At approximately $\alpha = 5$ deg, the wing encounters the beginning of massive shock-induced flow separation, and the magnitude of roll damping becomes less stable. As the angle of attack is further increased, CFD predicts a region of unstable roll damping between $\alpha = 7.75$ and $\alpha = 8.25$ deg. Above $\alpha = 8.25$ deg, the roll damping is stable. Regions of unstable roll damping such as this indicate that the aircraft could have abrupt roll-off motions, lightly damped wing rock, or other lateral issues. Because of the history of the F/A-18E program and the preproduction Super Hornet's problems with abrupt wing stall and random asymmetric roll-off behavior, the region of unstable roll damping shown in Fig. 4 is associated with well-documented unacceptable behavior.

The roll damping obtained from free-to-roll wind-tunnel tests are also plotted in Fig. 4. Recall that it is impossible to obtain pure C_{l_p} from the wind-tunnel tests. However, the roll damping from the wind-tunnel data also indicates a region of unstable roll damping, which occurs between $\alpha = 8.1$ and $\alpha = 8.8$ deg. It was not possible to obtain wind-tunnel data between these two angles of attack because the model's rolling motions became too violent at these conditions. Although there is a slight difference in the location of the unstable roll damping between CFD and the wind-tunnel data, the CFD data does predict the correct trend of the data. At angles of attack away from the region of unstable roll damping, the roll damping predicted by CFD compares well to that of the wind-tunnel data. Given all of the aforementioned differences regarding the estimation of roll damping from CFD and wind-tunnel tests, the correlation between CFD and the wind tunnel for this application is very good. An early prediction of lateral problems caused by loss of roll damping would be invaluable during an aircraft development program.

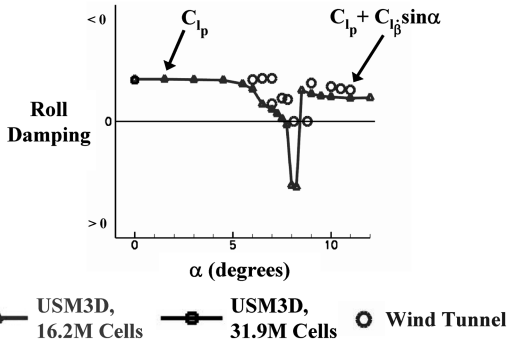

Fig. 4 Roll damping from wind tunnel and CFD as a function of angle of attack for the preproduction F/A-18E with 6/8/4 flaps at Mach 0.8, $Re_c = 3.9$ million and $p = 20$ deg/s.

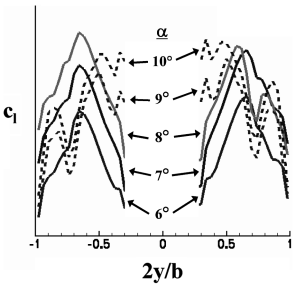

Fig. 5 Section-lift distribution predicted by CFD for the preproduction F/A-18E with 6/8/4 flaps at Mach 0.8, $Re_c = 3.9$ million and $p = 20$ deg/s.

In Fig. 5, the section-lift distribution on the wing is plotted for angles of attack between 6 and 10 deg for a roll rate of 20 deg/s (roll rate for right roll). At $\alpha = 6$ deg, the downgoing right wing is generating more lift than the left wing, generating a negative (opposing) rolling-moment coefficient and a stable roll-damping coefficient. As the angle of attack is increased to $\alpha = 7$ deg, the lift increases almost equally on both wings, resulting in a minimal resisting moment. As the angle of attack is increased to $\alpha = 8$ deg, the right wing abruptly loses lift at 72% span while the lift increases on the left wing. As a result, the left wing is generating more lift than the right wing, creating a positive (propelling) rolling-moment coefficient and the unstable roll-damping coefficient that is evident in Fig. 5. As the angle of attack increases to $\alpha = 9$ deg, the left wing also loses lift and generates less lift than the right wing, once again producing a stable roll-damping coefficient.

The section-lift distribution for roll rates of 0 and 20 deg/s for $\alpha = 8$ deg are plotted in Fig. 6. At this angle of attack, the deficit in lift at 72% span is clearly visible. On the aircraft, there is a leading-edge snag at 72% span. During the earlier abrupt-wing-stall program [24], flow separation emanating from the leading-edge snag was found to be a contributor to the abrupt wing stall experienced by the F/A-18E [25]. The results plotted in Figs. 4 and 6 show the impact of the separated flow on roll damping.

In Fig. 7, pressure contours and regions of reversed flow are shown on the upper surface of the wings for angles of attack between 6 and 9 deg. As the angle of attack is increased from 7 to 8 deg, the flow separation on the right wing moves forward to the leading-edge snag,

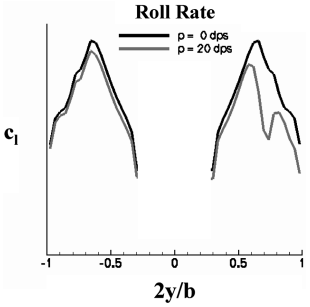

Fig. 6 Section-lift distribution predicted by CFD for the preproduction F/A-18E with 6/8/4 flaps at Mach 0.8, $Re_c = 3.9$ million and $\alpha = 8$ deg for $p = 0$ and 20 deg /s.

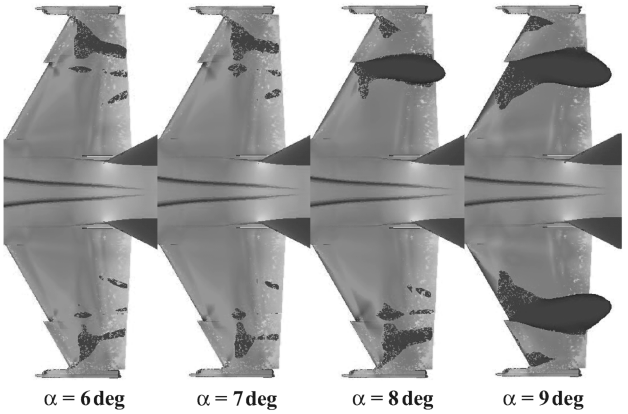

Fig. 7 Pressure contours and regions of reversed flow on the wing upper surface predicted by CFD for the preproduction F/A-18E with 6/8/4 flaps at Mach 0.8, $Re_c = 3.9$ million and $p = 20$ deg /s.

reducing the lift as shown in Fig. 6. As the angle of attack is increased to 9 deg, the flow separation on the left wing also moves forward to the leading-edge snag.

Experience has shown that aerodynamic roll damping near wing stall conditions is usually nonlinear as a function of roll rate. That is, when the roll rate exceeds a certain value, the downgoing wing becomes completely stalled, lift is somewhat restored, and the roll damping becomes less unstable, or even stable. To ensure that USM3D predicts the nonlinear trend of roll damping with roll rate, a roll rate of 90 deg /s was also considered for this configuration. In Fig. 8, the roll-damping coefficients predicted by CFD for roll rates of 20 and 90 deg /s are shown. As one would expect, the higher roll rate of 90 deg /s produces a stable roll-damping coefficient near $\alpha = 8$ deg, indicative of the expected nonlinear trend.

B. Preproduction F/A-18E with 6/8/4 Flaps at Flight Conditions

During the AWS program, numerous wind-tunnel tests were conducted that confirmed that the preproduction F/A-18E exhibited abrupt-wing-stall characteristics at wind-tunnel conditions [4,22]. In the previous section, it was shown that CFD was capable of predicting the unstable roll-damping characteristics of the preproduction F/A-18E at wind-tunnel conditions. The next step during this study was to determine if CFD could predict well-documented unstable roll-damping characteristics for the aircraft at flight conditions. The flight conditions used during these computations were Mach 0.8 at an altitude of 30,000 ft. The CFD calculations were performed with USM3D for a roll rate of 20 deg /s. In Fig. 9, the roll-damping coefficients are plotted as a function of angle of attack for the preproduction F/A-18E at wind-tunnel and flight conditions. These results indicate that the unstable roll-damping characteristics of the preproduction F/A-18E exist in flight, as well as in the wind tunnel. Based on these CFD results, the flight vehicle experienced a more unstable roll damping than the wind-tunnel model, at approximately the same angle of attack. The

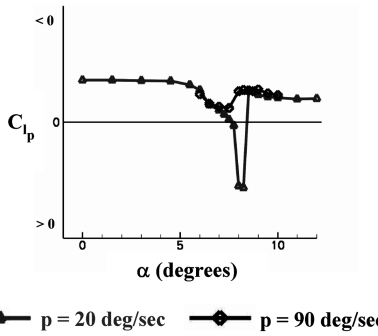

Fig. 8 Roll-damping coefficient from CFD as a function of angle of attack for the preproduction F/A-18E with 6/8/4 flaps at Mach 0.8, $Re_c = 3.9$ million and $p = 20$ and 90 deg /s.

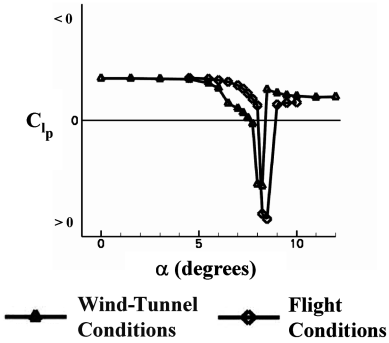

Fig. 9 Roll-damping coefficient from CFD at wind-tunnel and flight conditions as a function of angle of attack for the preproduction F/A-18E with 6/8/4 flaps at Mach 0.8 and $p = 20$ deg /s.

fact that CFD predicted unstable roll damping for both wind-tunnel and flight conditions for 6/8/4 flaps is an important result, as will become evident in a subsequent section of this paper.

C. Preproduction F/A-18E with 10/10/5 Flaps at Wind-Tunnel Conditions

During the preproduction F/A-18E flight test program, a modified flap schedule was implemented which did not completely eliminate the AWS problems, but did reduce the severity of the wing drop and its occurrence [26]. In an effort to model the effects of the more beneficial flap schedule, USM3D was used to predict the roll-damping characteristics of the preproduction F/A-18E with 10/10/5 flaps. The calculations were performed for Mach 0.8 at wind-tunnel conditions with a roll rate of 20 deg /s. The roll damping from CFD is compared with that from the wind-tunnel data in Fig. 10. Although the roll damping from the wind-tunnel data is stable, the results from CFD indicate that there are two regions of unstable roll damping. These regions occur at $\alpha = 6.5$ and $\alpha = 8.5$ deg. The positive values of roll damping from CFD would tend to indicate the presence of a severe wing-drop event. Although the values of roll damping from the wind tunnel are stable, wing rock was observed during the wind-tunnel test at $\alpha = 8$, 8.5, and 10 deg [22]. Once again, the comparison being made between the roll damping from CFD and the roll damping from the wind tunnel does not represent a one-to-one comparison. Although CFD may have overpredicted the severity of the wing-drop events in this case, it is important to realize that CFD did predict two distinct events, shifted in angle of attack from the wind-tunnel data.

The roll-damping coefficient is plotted as a function of angle of attack in Fig. 11 for the preproduction F/A-18E with 6/8/4 and 10/10/5 flaps. CFD predicts two wing-drop events for 10/10/5 flaps and only one event for 6/8/4 flaps. Based on the values of roll damping, CFD predicts that these two events for 10/10/5 flaps would be slightly less severe than what is present for 6/8/4 flaps. If these CFD results were all that were available to an aircraft designer, then the designer would have to conclude that the more aggressive flap setting

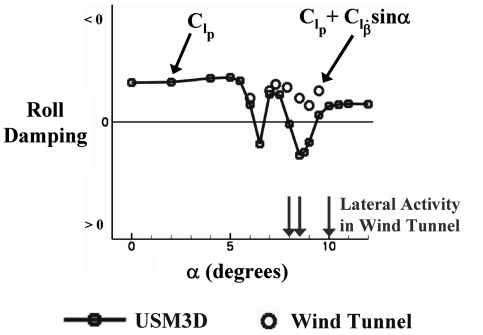

Fig. 10 Roll damping from wind tunnel and CFD as a function of angle of attack for the preproduction F/A-18E with 10/10/5 flaps at Mach 0.8, $Re_c = 3.9$ million and $p = 20$ deg /s.

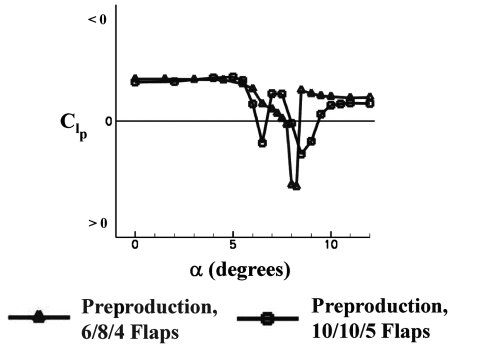

Fig. 11 Roll-damping coefficient from CFD as a function of angle of attack for the preproduction F/A-18E with 6/8/4 and 10/10/5 flaps at Mach 0.8, $Re_c = 3.9$ million and $p = 20$ deg /s.

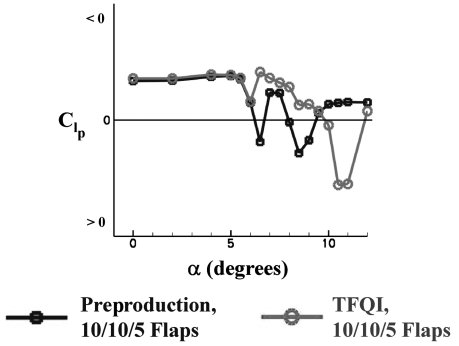

Fig. 12 Roll-damping coefficient from CFD as a function of angle of attack for the preproduction F/A-18E and the TFQI F/A-18E with 10/10/5 flaps at Mach 0.8, $Re_c = 3.9$ million and $p = 20$ deg /s.

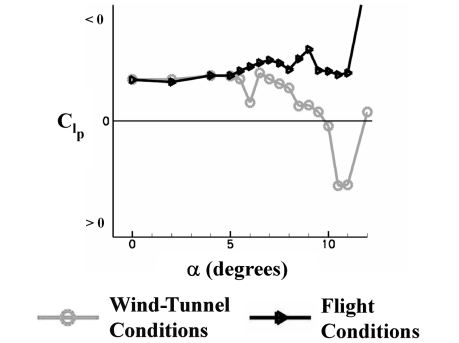

Fig. 13 Roll-damping coefficient from CFD at wind-tunnel and flight conditions as a function of angle of attack for the TFQI F/A-18E with 10/10/5 flaps at Mach 0.8 and $p = 20$ deg /s.

was not going to solve the AWS problem and the designer would have to look for another solution for solving the AWS problem.

D. F/A-18E with TFQI Modifications with 10/10/5 Flaps at Wind-Tunnel Conditions

After the change in flap schedule did not completely eliminate the AWS characteristics of the aircraft, the existing wing-fold fairing on the upper surface of the wing was replaced with a porous door [26]. The porous door was the result of a suggestion by one of the test pilots [26] and is currently included on the F/A-18E Super Hornets being delivered to the fleet today. Although the porous door solved the AWS problems of the aircraft, the porous door caused buffet that was not previously present [26] and was expected to increase the maintenance costs of the aircraft. As a result, other solutions to the AWS problem were investigated through the TFQI program. Through this program, other configuration changes were investigated as options to eliminating the AWS characteristics on the aircraft. After many exploratory flight tests, it was determined that the leading-edge snag should be replaced with a "sawtooth" geometry and a fence should be added to the upper surface of the wing to eliminate AWS on the aircraft. The sawtooth geometry was proposed, investigated, and patented by Darren Grove at Naval Air Systems Command and is discussed in [27]. This configuration, which does not include a porous door over the wing-fold fairing, can be seen in Fig. 2. These modifications are being included on the EA-18G Growler being designed today.

To evaluate the effectiveness of these TFQI changes to the Super Hornet, USM3D was used to predict the roll-damping characteristics of the aircraft at wind-tunnel conditions. The configuration was analyzed at Mach 0.8 at a roll rate of 20 deg /s. The roll-damping coefficients from CFD are plotted as a function of angle of attack in Fig. 12 for the preproduction F/A-18E with 10/10/5 flaps and the TFQI configuration (the preproduction F/A-18E with a sawtooth leading edge and a fence on the upper surface of the wing) with 10/10/5 flaps. The CFD results indicate that although the TQFI configuration did not eliminate the unstable roll-damping characteristics of the aircraft, it did move the instabilities to a higher angle of attack of 10.5 deg. Although there are no wind-tunnel data for this specific configuration, wind-tunnel data on a similar configuration with a sawtooth and two fences also increased the angle of attack of the instabilities [22]. Although it might appear from the results in Fig. 12 that the TFQI configuration could still have problems with roll damping, it is important to note that the instabilities have been pushed to an angle of attack beyond the 10/10/5 schedule vs angle of attack. The aircraft will never fly with 10/10/5 flaps at Mach 0.8 and $\alpha = 10.5$ deg and, as a result, the flight vehicle will not experience the lateral instability that is predicted by CFD at $\alpha = 10.5$ deg.

E. F/A-18E with TFQI Modifications with 10/10/5 Flaps at Flight Conditions

USM3D was also used to predict the roll-damping characteristics of the TFQI aircraft with 10/10/5 flaps at flight conditions. These calculations were performed at Mach 0.8, at an altitude of 30,000 ft, and a roll rate of 20 deg /s. The roll-damping coefficients predicted by CFD are plotted as a function of angle of attack for the TFQI configuration at wind-tunnel and flight conditions in Fig. 13. In this figure, it can be seen that the roll-damping coefficients are stable at flight conditions for angles of attack between 0 and 12 deg. At wind-tunnel conditions, unstable roll damping exists at 10.5 and 11 deg angle of attack. Recall from Fig. 9 that the preproduction F/A-18E with 6/8/4 flaps had unstable roll damping at both wind-tunnel and flight conditions. For the case of the TFQI configuration with 10/10/5 flaps, the unstable roll damping that was present at wind-tunnel conditions is eliminated at the flight conditions. This intriguing result introduces the issue of how to scale flow-control devices such as fences and sawtooths for wind-tunnel models to more properly simulate flight conditions. This result is considered to be one of the more important finds of the current study, and certainly worthy of further studies by the CFD community. Other aircraft programs have

also investigated flow-control devices that did not scale aerodynamically between wind-tunnel and flight conditions [28].

VII. Summary

The goal of this study was to conduct exploratory investigations to assess the ability of CFD to predict the roll-damping characteristics of the F/A-18E Super Hornet at transonic speeds. The CFD calculations were performed blind, without prior knowledge of the existing wind-tunnel data. Before initiating the computations, modifications were made to the USM3D flow solver that made it possible to estimate roll damping. The CFD calculations were performed on three different F/A-18E configurations at Mach 0.8. Wind-tunnel data existed for two of the configurations, which made it possible to validate the CFD calculations. The roll damping for both wind-tunnel and flight conditions were evaluated for two of the configurations, testing the ability of CFD to predict the effect of Reynolds number on roll damping. For one of the configurations, the roll rate was varied to confirm that CFD predicted the correct trend of roll damping with roll rate. In the end, CFD was shown to be a valuable tool for assessing the roll-damping characteristics of an aircraft.

This study represents the final phase of CFD calculations being performed as part of the CST portfolio. The first phase involved longitudinal and lateral/directional stability-and-control predictions on the preproduction F/A-18E at transonic speeds, and the second phase involved predicting the longitudinal stability-and-control characteristics of the preproduction F/A-18E with neutral and full nose-down control at low-speed, high-angle-of-attack conditions. Based on these results, considerable promise exists for the application of current CFD methods for future high-performance aircraft. Such applications would allow the designer to augment his existing toolbox to extrapolate experimental predictions to higher values of Reynolds number, provide flow diagnostic capability for stability-and-control problems, and provide analysis capabilities where wind-tunnel techniques are not available. Additional requirements for stability-and-control analysis such as aircraft dynamic-motion effects on aerodynamics might be particularly fruitful areas of research in the near future. In addition, other aircraft configurations which use different geometry (such as wing sweep) need to be analyzed to assess the general applicability of the current results and to further demonstrate that CFD is a viable predictive tool for stability-and-control engineers.

Acknowledgments

The author would like to gratefully acknowledge the funding that was granted for this study by the High Performance Computing Modernization Office through the Collaborative Simulation and Testing portfolio. In addition, the author would like to thank David Findlay and James Chung for their guidance and insight. Also, the author would like to thank the High Performance Computing Modernization Office for the many hours of computer time that was necessary to complete this computational study. Finally, the author acknowledges the advice and guidance of the following individuals: Steve Hynes and Alex Kokolios of Naval Air Systems Command; Robert Hall, Neal Frink, and Mike Fremaux of NASA Langley Research Center; Joseph Chambers, retired from NASA Langley Research Center and consultant; and Mohagna Pandya of Analytical Services and Materials, Inc.

References

[1] Chambers, J. R., and Hall, R. M., "Historical Review of Uncommanded Lateral-Directional Motions at Transonic Conditions," *Journal of Aircraft*, Vol. 41, No. 3, 2004, pp. 436–447.

[2] Green, B. E., and Chung, J. J., "Transonic Computational Fluid Dynamics Calculations on Preproduction F/A-18E for Stability and Control," *Journal of Aircraft*, Vol. 44, No. 2, 2007, pp. 420–426. doi:10.2514/1.22846

[3] Green, B. E., "Computational Prediction of Nose-Down Control for the Pre-Production F/A-18E at High Angles of Attack," AIAA Paper 2007-6724, Aug. 2007.

[4] Owens, D. B., Capone, F. J., Hall, R. M., Brandon, J. M., and Chambers, J. R., "Transonic Free-to-Roll Analysis of Abrupt Wing Stall on Military Aircraft," *Journal of Aircraft*, Vol. 41, No. 3, 2004, pp. 474–484.

[5] Frink, N. T., Pirzadeh, S. Z., Parikh, P. C., Pandya, M. J., and Bhat, M. K., "NASA Tetrahedral Unstructured Software System," *Aeronautical Journal*, Vol. 104, No. 1040, 2000, pp. 491–499.

[6] Pirzadeh, S., "Unstructured Viscous Grid Generation by Advancing-Layers Method," *AIAA Journal*, Vol. 32, No. 8, 1994, pp. 1735–1737.

[7] Löhner, R., and Parikh, P. C., "Three-dimensional Grid Generation by the Advancing Front Method," *International Journal for Numerical Methods in Fluids*, Vol. 8, No. 10, 1988, pp. 1135–1149. doi:10.1002/fld.1650081003

[8] Samareh, J., "GridTool: A Surface Modeling and Grid Generation Tool ," *Proceedings of the Workshop on Surface Modeling, Grid Generation, and Related Issues in CFD Solutions*, NACA CP-3291, NASA Lewis Research Center, Cleveland, OH, May 1995, p. 12.

[9] Frink, N. T., "Tetrahedral Unstructured Navier-Stokes Method for Turbulent Flows," *AIAA Journal*, Vol. 36, No. 11, 1998, pp. 1975–1982.

[10] Pandya, M. J., Frink, N. T., Abdol-Hamid, K. S., and Chung, J. J., "Recent Enhancements to USM3D Unstructured Flow Solver for Unsteady Flows," AIAA Paper 2004-5201, Aug. 2004.

[11] Pandya, M. J., Abdol-Hamid, K. S., Campbell, R. L., and Frink, N. T., "Implementation of Flow Tripping Capability in the USM3D Unstructured Flow Solver," AIAA Paper 2006-0919, Jan. 2006.

[12] Pandya, M. J., Frink, N. T., and Noack, R. W., "Progress Toward Overset-Grid Moving Body Capability for USM3D Unstructured Flow Solver," AIAA Paper 2005-5118, June 2005.

[13] Spalart, P., and Allmaras, S. A., "One-Equation Turbulence Model for Aerodynamic Flows," AIAA Paper 1992-0439, Jan. 1992.

[14] Jones, W. P., and Launder, B. E., "Prediction of Laminarization with a Two-Equation Model of Turbulence," *International Journal of Heat and Mass Transfer*, Vol. 15, No. 2, 1972, pp. 301–314. doi:10.1016/0017-9310(72)90076-2

[15] Sarkar, S., Erlebacher, G., Hussaini, M. Y., and Kreiss, H. O., "Analysis and Modeling of Dilatational Terms in Compressible Turbulence," *Journal of Fluid Mechanics*, Vol. 227, June 1991, pp. 473–495. doi:10.1017/S0022112091000204

[16] Menter, F. R., "Improved Two-Equation k-omega Turbulence Models for Aerodynamic Flows," NASA TM-103975, Oct. 1992.

[17] Girimaji, S. S., "Fully-Explicit and Self-Consistent Algebraic Reynolds Stress Model," International Council of the Aeronautical Sciences Rept. 95-82, 1995.

[18] Shih, T-H., Zhu, J., and Lumley, J. L., "New Reynolds Stress Algebraic Model," NASA TM-166614, Inst. for Computational Mechanics 94-8, 1994.

[19] Abdol-Hamid, K. S., Frink, N. T., Deere, K. A., and Pandya, M. J., "Propulsion Simulations Using Advanced Turbulence Models with the Unstructured-Grid CFD Tool, TetrUSS," AIAA Paper 2004-0714, Jan. 2004.

[20] Karypis, G., and Kumar, V., "Fast and High Quality Multilevel Scheme for Partitioning Irregular Graphs," *SIAM Journal on Scientific Computing*, Vol. 20, No. 1, 1998, pp. 359–392. doi:10.1137/S1064827595287997.

[21] Park, S. H., and Kwon, J. H., "Navier–Stokes Computation of Pitch-Damping Coefficients Using Steady Coning Motions," *Journal of Spacecraft and Rockets*, Vol. 41, No. 5, 2004, pp. 754–761.

[22] Owens, D. B., McConnell, J. K., Brandon, J. M., and Hall, R. M., "Transonic Free-to-Roll Analysis of the F/A-18E and F-35 Configurations," AIAA Paper 2004-5053, Aug. 2004.

[23] Capone, F. J., Owens, D. B., and Hall, R. M., "Development of a Free-To-Roll Transonic Test Capability," *Journal of Aircraft*, Vol. 41, No. 3, 2004, pp. 456–463.

[24] Hall, R. M., and Woodson, S. H., "Introduction to the Abrupt Wing Stall Program," *Journal of Aircraft*, Vol. 41, No. 3, 2004, pp. 425–435.

[25] Green, B. E., and Ott, J. D., "F/A-18C to E Wing Morphing Study for the Abrupt-Wing-Stall Program," *Journal of Aircraft*, Vol. 42, No. 3, 2005, pp. 617–626.

[26] Traven, R., Hagan, J., and Niewoehner, R., "Solving Wing Drop on the F/A-18E Super Hornet, 1998 Report to the Aerospace Profession," *Proceedings of the 42nd Symposium Aerospace and High Technology Database*, Society of Experimental Test Pilots, Sept. 1998, pp. 67–84.

[27] Grove, D. V., "Computational Fluid Dynamics Study of Abrupt Wing Stall Phenomena on an F/A-18E Using the Patented Sawtooth Leading Edge Flap," AIAA Paper 2006-0854, Jan. 2006.

[28] Bore, C. L., "Post-Stall Aerodynamics of the Harrier GR1," *Fluid Dynamics of Aircraft Stalling*, AGARD CP-102, 1972, pp. 19–5.